Polymorph transformation in a mixed-stacking nickel-dithiolene complex with the derivative of 4,4′-bipyridinium

Yan Gao,[a] Lei Xu,[a] Zi-Heng Feng,[a] Yin Qian,*[a] Zheng-Fang Tian,[b] Xiao-Ming Ren*[a,c]

[a]State Key Laboratory of Materials-Oriented Chemical Engineering and College of Chemistry and Molecular Engineering, Nanjing Tech University, Nanjing 211816, P. R. China

[b]Hubei Key Laboratory of Processing and Application of Catalytic materials, Huanggang Normal University, Huanggang, 438000, P. R. China

[c]State Key Laboratory of Coordination Chemistry, Nanjing University, Nanjing 210093, P. R. China

Email: yinqian@njtech.edu.cn (Y.Q.); xmren@njtech.edu.cn (X.M.R.)

Contents

Experimental section

Materials

All reagents and chemicals were purchased from commercial sources and used directly. Disodium maleonitriledithiolate (Na_2mnt),[1] 1,1'-dibutyl-4,4'-bipyridinium dibromide ($[C_4$-4, 4'-BiPy$]Br_2$)[2] were prepared following the published procedures.

Synthesis of $[C_4$-4, 4′-BiPy$][Ni(mnt)_2]$ (1-g)

$[C_4$-4,4′-Bipy$][Ni(mnt)_2]$ (**1**-g): Na_2mnt (372 mg, 2 mmol) and $NiCl_2{\cdot}6H_2O$ (237 mg, 1 mmol) were mixed under stirring with 100 mL H_2O at ambient temperature, subsequently, a solution of $[C_4$-4, 4'-BiPy$]Br_2$ (430 mg, 1 mmol) with 30 mL H_2O was added to the mixture. The precipitate was immediately formed, and the mixed solution was vigorously stirred for 10 min. and then filtered off, washed with 15 mL of H_2O (3×5 mL). The crude product was collected by suction and dried in an oven at 40°C for 4h to give light green microcrystals, with yield of ~84% (calc. based on $NiCl_2{\cdot}6H_2O$). Anal. Calc. for $C_{26}H_{26}N_6S_4Ni$ (**1**-g): C, 51.24; H, 4.30; N, 13.79%. Found: C, 51.13; H, 4.30; N, 13.94%. **1**-g underwent immersion in MeOH and was subjected to ultrasonic treatment for half hour, yielding a microcrystalline sample that appeared red in color (denoted as **1**-r), and microanalysis found: C, 51.21; H, 4.28; N, 14.08%.

The single crystals suitable for X-ray structure analysis were grown by diffusion method in a sealed test tube, i.e., the solution of **1**-r in 3 mL of DMF and 10 mL EtOH are placed on the bottom and top of a test tube, respectively. This tube was sealed at ambient temperature, and the plate-shaped crystals of **1**-r were obtained for ~10 days.

Physical measurements

Elemental analyses for C, H, and N were performed on an Elementar Vario EL III analytic instrument. IR spectra in 4000–450 cm^{-1} were recorded on Bruker Tensor FTIR instrument that was equipped with an attenuated total reflection cell (Harrick) (ATR-FTIR). Powder X-ray diffraction (PXRD) data were collected on a MiniFlex600 X-ray diffractometer with Cu K_α (λ = 1.5404 Å) radiation at ambient temperature.

Thermogravimetric (TG) analyzer experiments were performed using a

simultaneous SDT 2960 thermal, the sample was held in a platinum pan under nitrogen flow in the rate of 100 mL min^{-1} and heated at a ramping rate of 20 °C min^{-1} from 303 to 1073 K (from 30 to 800 °C). Differential scanning calorimeter (DSC) experiments were carried out on Shimadzu DSC-60 differential scanning calorimeter in the temperature range of 186-523 K (from –87 to 250 °C).

Dielectric constant and loss measurements were carried out using Concept 80 system (Novo control, Germany) in the ranges of 1-10^7 Hz and 173-403 K; the powdered sample of **1**-r was pressed to a pellet with a thickness of ca. 1.216 mm and a diameter of 7.0 mm (an area of 38.5 mm^2) under a static pressure of 8 MPa for 5 min., which two surfaces were gold-plated, such pellet was sandwiched by the copper electrodes for dielectric measurements, and the temperatures range from 173 to 473 K and the alternating current (AC) frequencies change from 1 to 10^7 Hz. Solid-state UV-vis-NIR absorption spectra were recorded on a Shimadzu UV3600PLUS equipped with Integrating Spheres.

X-Ray single crystallography

Single-crystal X-ray diffraction data were collected on a Bruker D8 QUEST Apex III CCD area detector diffractometer with graphite-monochromated Mo K_α radiation (λ = 0.71073 Å) at room temperature. Data reduction and absorption correction were performed with the SAINT[3] and SADABS[4] software packages, respectively. The crystal structure was solved by direct method and refined on F^2 using full matrix least-squares method with SHELXTL package.[5] All hydrogen atoms were placed at the calculated positions and refined as riding on their parent atoms with fixed isotropic displacement parameters. X-ray diffraction data collection, structure refinement, and crystallography are summarized in Table S1.

Table S1. Crystal data and structure refinement parameters for **1**-r

Chemical formula	$C_{26}H_{26}N_6NiS_4$	$C_{26}H_{26}N_6NiS_4$
CCDC number	2311213	2311215
Formula weight	609.48	609.48
Temperature (K)	100	296
Wavelength (Å)	0.71073	0.71073
Crystal system	triclinic	monoclinic
Space group	*P*–1	*P*2/c
a (Å)	7.1650(7)	8.864(2)
b (Å)	9.2160(8)	8.089(2)
c (Å)	21.1039(18)	20.473(5)
α (°)	94.597(3)	90.00
β (°)	94.082(3)	98.664(9)
γ (°)	93.219(3)	90.00
V (Å^3) / Z	1382.9(2)	1451.1(7)
D_{calc} (g/cm^3)	1.464	1.395
Abs. coefficient (mm^{-1})	1.031	0.983
F(000)	632	632
θ range for data collection	2.221–26.405	2.32–26.40
Index range	-8<h<8	-11<h<11
	-10<k<11	-10<k<10
	-26<l<26	-25<l<24
Reflections collected	15728	12093
Independent reflections	5634	2928
R_{int}	0.0615	0.0852
Refinement on F^2	Full-matrix least-squares	Full-matrix least-squares
Data / restraints / parameters	5634 / 0 / 337	2928 / 0 / 169
Goodness-of-fit on F^2	1.034	1.013
Final R indices [I > 2σ(I)]	0.0447	0.0540
R indices (all data)	0.0680	0.1246
Residual (eÅ^{-3})	0.663/-0.682	0.230/-0.249

Table S2. Enthalpy and entropy changes of phase transitions in **1**-g and **1**-r, together with the peak temperature of thermal anomalies

1-g												
Mode	T_{peak}/K			ΔH/kJ mol^{-1}			ΔS/J mol^{-1} K^{-1}			N_2/N_1		
Heating	1st	2nd	3rd	1st	2nd	3rd	1st	2nd	3rd	1st	2nd	3rd
	399.0	400.7	400.1	8.3	6.2	6.0	20.8	15.5	15.0	12.2	6.5	6.1
Cooling	1st	2nd	3rd	1st	2nd	3rd	1st	2nd	3rd	1st	2nd	3rd
	366.0	363.1	362.5	8.7	7.7	7.2	23.8	21.2	19.8	17.5	12.8	10.8
1-r												
Heating	1st	2nd	3rd	1st	2nd	3rd	1st	2nd	3rd	1st	2nd	3rd
	274.2	402.1	402.5	1.05	4.6	4.6	3.8	11.4	11.4	1.58	3.9	3.9
Heating	1st	2nd	3rd	1st	2nd	3rd	1st	2nd	3rd	1st	2nd	3rd
	494.8	480.2	479.1	16.6	2.1	2.1	33.6	4.4	4.4	56.9	1.7	1.7
Cooling	1st	2nd	3rd	1st	2nd	3rd	1st	2nd	3rd	1st	2nd	3rd
	380.2	381.8	381.8	6.8	7.2	7.2	18.0	18.8	18.8	8.7	9.6	9.6

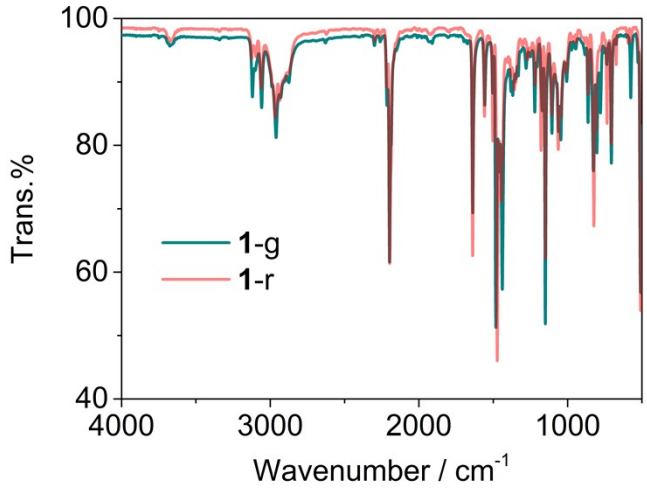

Figure S1. IR spectrum of **1**-r and **1**-g in 4000–500 cm^{-1}.

The most intense vibrational band of $\nu_{C\equiv N}$ (less than 2200 cm^{-1}) indicates that the valence of anion species is –2, band located at 735.7 cm^{-1} is assigned to the number of alkyl chain length is less than three carbon atoms.

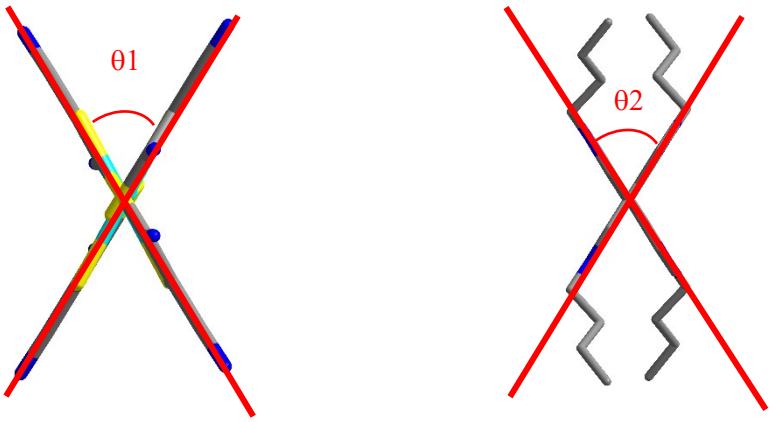

Figure S2. Schematic illustration for the dihedral angles between the mean-molecular planes of anions as well as between the mean-molecular planes of bipyridyl rings in the neighboring mixed-stacking columns of **1**-r. θ1 = 57.83° at 296 K, 61.19° at 100 K; θ_2 = 63.72° at 296 K, 72.74° at 100 K.

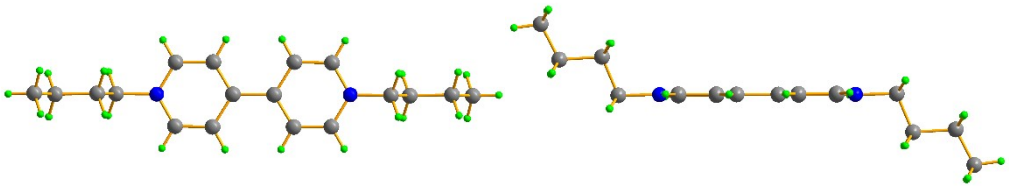

Figure S3. Top and side views of C_4-4,4′-Bipy^{2+} cation in the crystal structure of **1**-r at 296 K (in the high-temperature phase), where the butyl chains show all-trans conformation.

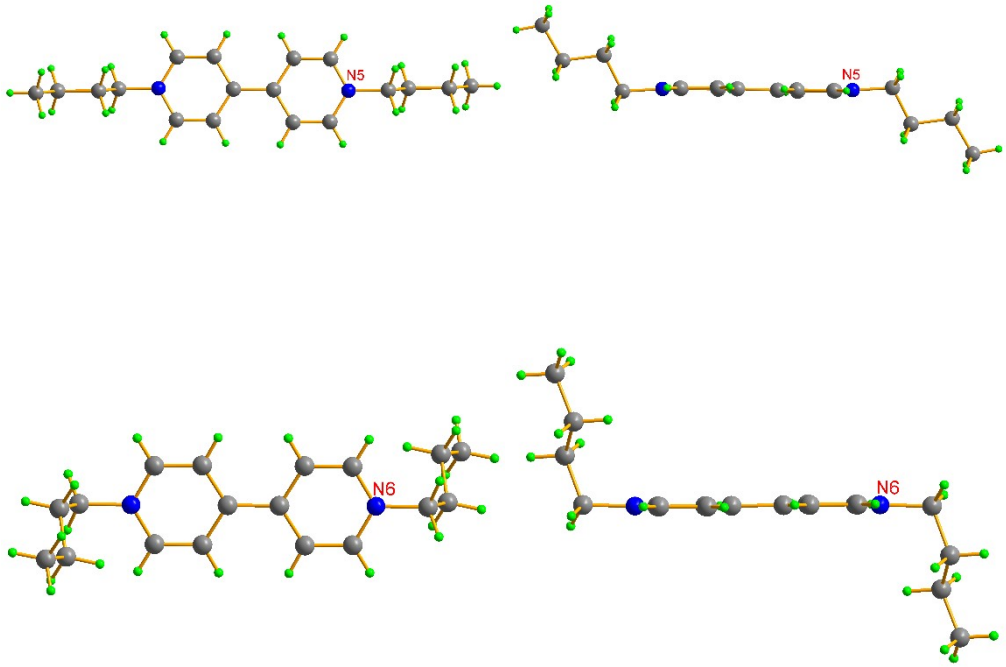

Figure S4. Top and side views of two crystallographically different C_4-4,4′-Bipy^{2+} cations in the crystal structure of **1**-r at 100 K (in the low-temperature phase), where the butyl chains show all-trans conformation.

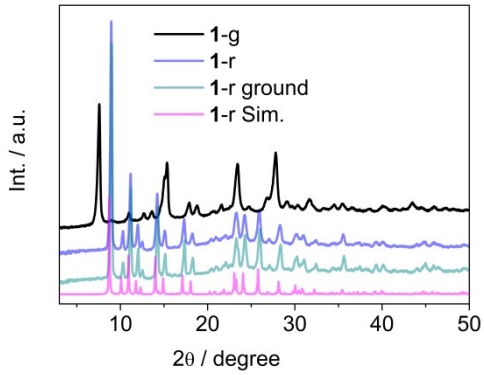

Figure S5. Experimental PXRD patterns of **1**-g, **1**-r and **1**-r ground together with the simulated PXRD pattern of **1**-r.

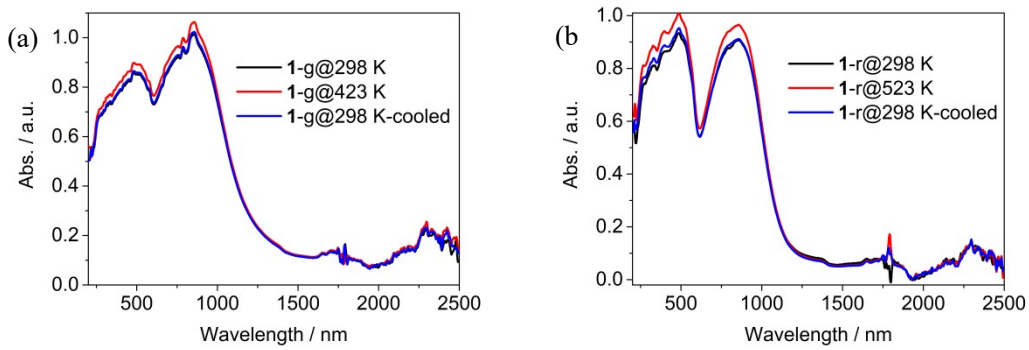

Figure S6. Variable-temperature UV-visible-near IR spectra of (a) **1**-g and (b) **1**-r.

Figure S7. Variable-temperature images of **1**-g, displaying the sequence of temperature changes following the direction of the arrow. **1**-g is a poor conductor of heat, leading to non-uniform heating of its constituent particles. Consequently, certain particles in the sample back to 298 K attain higher temperatures than others, manifesting as a slight red hue in some powdered particles.

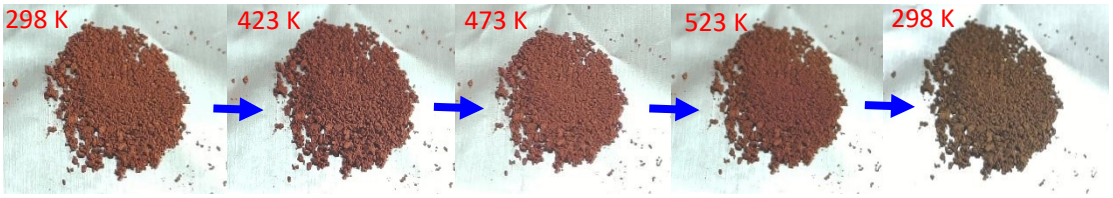

Figure S8. Variable-temperature images of **1**-r, displaying the sequence of temperature changes following the direction of the arrow. **1**-r is a poor conductor of heat, leading to non-uniform heating of its constituent particles. Consequently, certain particles in the sample back to 298 K attain higher temperatures than others, manifesting as a slight red hue in some powdered particles.

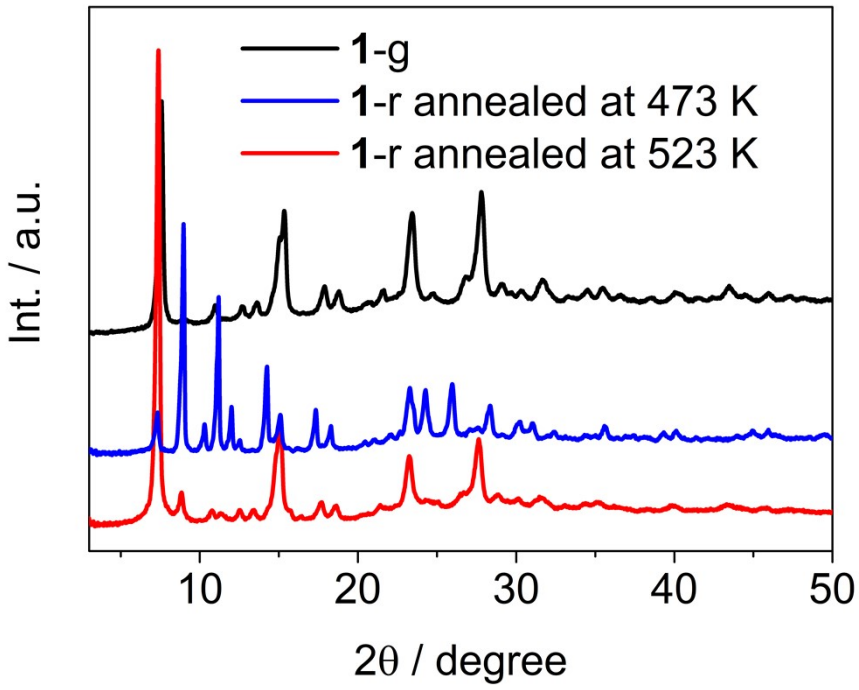

Figure S9. PXRD patterns of **1**-g, **1**-r annealed at 473 and 523 K and the measurement performed at room temperature.

References

1. A. Davidson, H. R. Holm, Metal complexes derived from cis-1,2-dicyano-1,2-ethylenedithiolate and bis(trifluoromethyl)-1, 2-dithiete, *Inorg. Synth.*, 1967, **10**, 8–26.
2. H. B. Duan, X. M. Ren, L. J. Shen, W. Q. Jin, Q. J. Meng, Z. F. Tian, S. M. Zhou, A low-dimensional molecular spin system with two steps of magnetic transitions and liquid crystal property, *Dalton Trans.*, 2011, **40**, 3622–3630.
3. Bruker, APEX 2, SAINT, XPREP, Bruker AXS Inc., Madison, Wisconsin, USA, 2007.
4. Bruker, SADABS, Bruker AXS Inc., Madison, Wisconsin, USA, 2001.
5. Sheldrick, G. M. *SHELXS-2014*, Program for the Solution and Refinement of Crystal Structures, University of Göttingen, Göttingen, Germany, 2014.